SERS

Plasma Modified MoS_2 Nanoflakes for Surface Enhanced Raman Scattering

Linfeng Sun, Hailong Hu, Da Zhan, Jiaxu Yan, Lei Liu, Jefri S. Teguh, Edwin K. L. Yeow, Pooi See Lee, and Zexiang Shen**

Molybdenum disulfide (MoS_2), a new type of two dimensional (2D) layered transition metal dichalcogenides with its unique electronic, optical, and mechanical properties, has been investigated and applied widely in transistors,[1–3] gas sensors,[4,5] lithium ion batteries,[6–8] spintronics,[9,10] hydrogen production,[11,12] and dry lubricant, etc.[13] Furthermore, the recent works reported that when MoS_2 exposed to triethylamine, it can be used effectively as a chemical sensor and exhibit a highly selective reactivity to a wide range of analytes due to the charge redistribution induced by the perturbations on the MoS_2 surface.[14] Thus, surface modification leads to the strong interaction between MoS_2 and detected molecules. Some experiments have also been reported to tune the activity of substrate for surface enhanced Raman scattering (SERS), such as nitrogen doping enhanced molecule sensing,[15] UV/Ozone oxidized treatment with an improved detection sensitivity,[16] and fluorinate function on graphene oxide by CF_4 plasma to increase molecule detection.[17] In this work, we observe an improved Raman enhancement of Rhodamine 6G (R6G) molecules deposited on oxygen-plasma treated MoS_2 (OT-MoS_2) and argon-plasma treated MoS_2 (AT-MoS_2) nanoflakes. Compared with the intensity of Raman spectra of R6G on pristine MoS_2 (P-MoS_2) nanoflakes, it is found that the Raman intensities of R6G molecules on both oxygen and argon plasma treated MoS_2 (T-MoS_2) are enhanced more than one order. The introduction of defects in T-MoS_2 samples changes the local surface properties of MoS_2 nanoflakes, such as creating the local dipoles which give rise to the enhancement of Raman signals of R6G molecules and adsorbance of the oxygen in ambient air to dope holes in MoS_2, resulting in the enhanced charge transfer effect between R6G and MoS_2. Furthermore, the layer-dependent Raman enhancement (R6G) mechanism on MoS_2 nanoflakes is explained in detail by comparing the enhancement behaviors on both supported and suspended MoS_2 nanoflakes with different layer numbers.

High crystalline quality MoS_2 nanoflakes were mechanically exfoliated from commercial MoS_2 crystal (SPI Supplies), and then transferred to a p-type silicon wafer coated by a 285 nm thick silicon oxide (SiO_2) layer. The R6G deposited on P-MoS_2 sample does not show obvious Raman enhancement. In contrast, the R6G molecules deposited on T-MoS_2 present dramatically enhanced Raman intensities. The comparison of Raman intensities of R6G molecules that deposited on SiO_2/Si substrate, P-MoS_2, OT-MoS_2 and AT-MoS_2 is carefully analyzed. **Figure 1**a gives a schematic illustration of R6G molecules deposited on 1L P-MoS_2, OT-MoS_2 and AT-MoS_2, respectively. Figure 1b shows the Raman spectra of R6G molecules deposited on different substrates mentioned in Figure 1a. For identifying the fluorescence quenching effect of MoS_2, the Raman spectrum of R6G deposited directly on SiO_2/Si is also given. All the spectra were measured with a 532 nm laser (2.33 eV) and the laser power is below 0.5 mW to avoid laser induced local heating effects. From Figure 1b, it can be seen that the Raman signal of R6G on 1L P-MoS_2 sample can be almost ignored despite the fact that the fluorescence background is suppressed. On the other hand, the Raman signals of R6G molecules on both OT-MoS_2 and AT-MoS_2 samples are enhanced obviously with the further suppression of fluorescence background of R6G compared to that of R6G on P-MoS_2. According to the previous reports, structural disorder can usually introduce local dipoles leading to

L. F. Sun, Dr. H. L. Hu, Dr. D. Zhan,
J. X. Yan, Prof. Z. X. Shen
Division of Physics and Applied Physics
School of Physical and Mathematical Sciences
Nanyang Technological University
637371, Singapore
E-mail: physicsor@gmail.com; zexiang@ntu.edu.sg
Prof. Z. X. Shen
Centre for Disruptive Photonic Technologies
School of Physical and Mathematical Sciences
Nanyang Technological University
637371, Singapore
Dr. H. L. Hu, Dr. D. Zhan, Prof. P. S. Lee, Prof. Z. X. Shen
Division of Materials Technology
School of Materials Science and Engineering
Nanyang Technological University
639798, Singapore
Prof. L. Liu
Key Laboratory of Luminescence and Applications
CIOMP, Chinese Academy of Sciences
No.3888 Dongnanhu Road, Changchun 130033
People's Republic of China
J. S. Teguh, Prof. E. K. L. Yeow
Division of Chemistry and Biological Chemistry
School of Physical and Mathematical Sciences
Nanyang Technological University,
Singapore 637371, Singapore

DOI: 10.1002/smll.201300798

NANO MICRO small

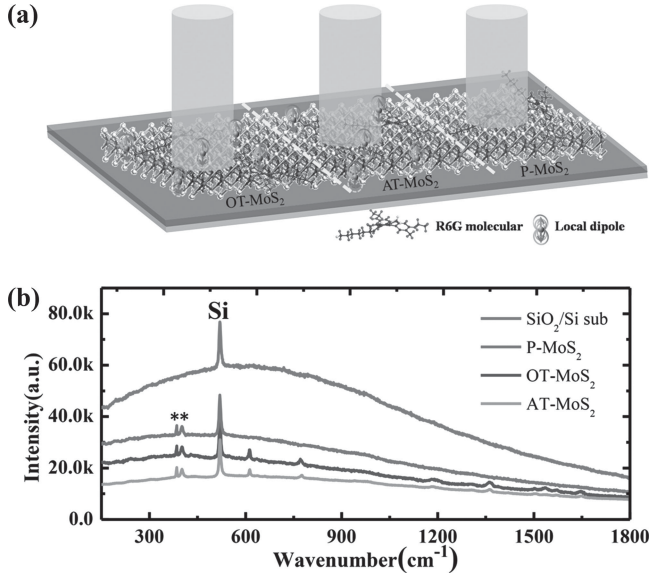

Figure 1. a) Schematic illustration of the R6G molecules on 1L P-MoS_2 and OT(AT)-MoS_2, respectively; b) Raman spectra of R6G molecules on SiO_2/Si substrate, 1L P-MoS_2 and OT(AT)-MoS_2. The Raman peaks originate from MoS_2 denoted by asterisks (*).

the improved SERS effect.[15–17] As 1L MoS_2 is only ~0.65 nm thick, its structure is easily modified during plasma treatment (bombardment) process, thus the generated structural disorder induced local dipole in 1L MoS_2 should be the driven force for enhancing Raman signals of R6G molecules. Next, we will reveal the SERS mechanism by studying the surface properties of the plasma treated MoS_2 samples in detail.

Raman and photoluminescence (PL) spectra of P-MoS_2 and OT(AT)-MoS_2 are shown in **Figure 2**, From the Raman spectra, it can be seen obviously that the frequency difference between the two prominent Raman modes, E^1_{2g} and A_{1g}, becomes larger for the treated samples by oxygen (argon) plasma. Eda et al. has observed similar effect on chemically exfoliated single layer MoS_2 nanoflakes.[18] CVD grown MoS_2 nanoflakes also show a larger frequency difference between these two predominant peaks compared to that of the MoS_2 prepared by mechanical exfoliation.[19,20] All of them ascribed this phenomenon to the disordered surface structure of MoS_2 nanoflakes. Figure S1 (Supporting information) shows the atomic force microscopy (AFM) images of 1L P-MoS_2 and OT(AT)-MoS_2 nanoflakes. It can be seen that the surface of OT(AT)-MoS_2 samples becomes more rough compared to the surface of P-MoS_2 as shown by the height profiles in the inset of Figure S1, and the mean square roughness values for P-MoS_2, OT-MoS_2 and AT-MoS_2 are 0.171, 0.543 and 0.621 nm respectively. It indicates that the structural disorder is introduced into the MoS_2 nanoflakes during plasma treatment process.[18,21] Furthermore, by investigating the variation of PL spectra of 1L P-MoS_2 and OT(AT)-MoS_2 nanoflakes shown in Figure 2b, it can be seen that the PL peak positions of both OT- and AT-MoS_2 show obvious blueshift compared to those of P-MoS_2. We propose that the blueshift of PL for T-MoS_2 is due to the band filling effect, which has been reported in disordered InN microcrystals,[22] CdSe,[23] and AlGaN/GaN.[24,25] As structure disorder in 2D material is normally a chemically unstable site, it is favorable to be adsorbed by oxygen in ambient air,[26] and hence the adsorption of oxygen gives rise to the p-doping effect to MoS_2 nanoflakes because of the strong electronegativity of oxygen,[27,28] which means that the adsorption of oxygen decreases the electron occupation level at around the top of valence band. As a consequence, the blueshift of PL peak is observed because the holes filling at the top of valance band provides the additional electronic transition pathways for increased PL emission energy. It is worth mentioning that once the OT(AT)-MoS_2 samples were put into the vacuum chamber (~1-x10^{-2} mbar), the in-situ measurement probed that the blueshifted PL peak of T-MoS_2 shows redshift, and the peak position recovers back to the position as similar as that of pristine MoS_2 sample. It indicates that the physically adsorbed O_2 is desorbed in vacuum environment. Interestingly, the PL peak position shows an obvious blueshift again once the samples re-exposed in ambient air (**Figure 3**). This vacuum experiment confirms that the oxygen in ambient air is favorable to be weakly adsorbed at defect sites of T-MoS_2, and it can be desorbed easily in vacuum.[26]

To explore the interaction between the R6G molecules and both P-MoS_2 and T-MoS_2, we carried out the PL spectra

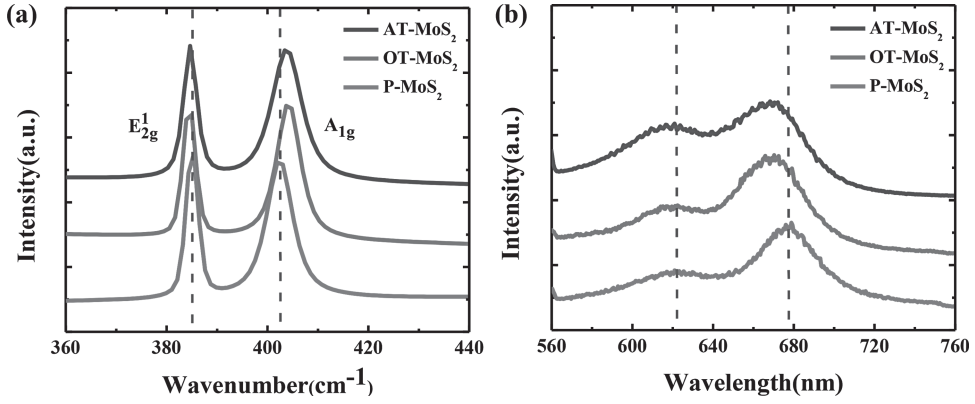

Figure 2. a) Raman spectra and b) PL spectra of 1L P-MoS_2 and OT(AT)-MoS_2. The blue dashed lines represent the Raman (a) and PL (b) peak positions of 1L P-MoS_2 samples, respectively.

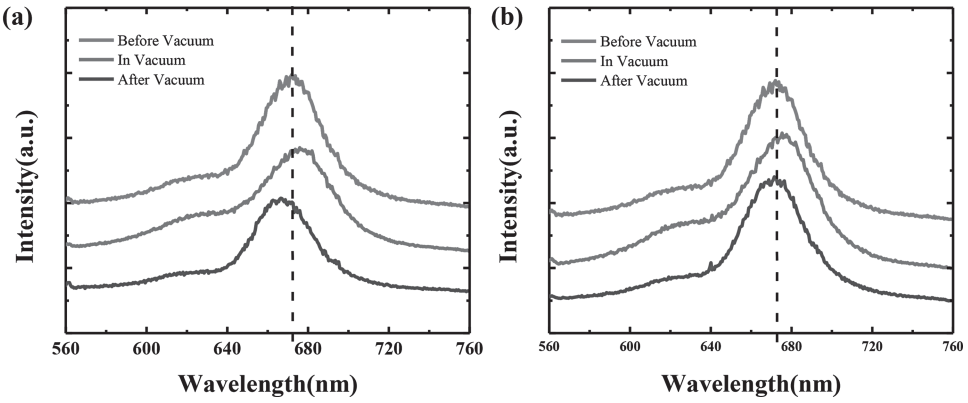

Figure 3. PL measurements for 1L (a) OT-MoS_2 and (b) AT-MoS_2 samples. The red lines represent the samples measured in ambient air before putting into the vacuum chamber; the green lines represent the samples measured in vacuum at 1×10^{-2}mbar; the blue lines represent the samples re-exposed to the ambient air after removing the vacuum.

study on these samples. It is worth noting that as the surface properties of AT-MoS_2 and OT-MoS_2 do not present obvious difference, thus we will only use OT-MoS_2 on behalf of T-MoS_2 in the following experiments. As shown in Figure S2, it is found that after the deposition of R6G molecules, the blueshifted PL peak position of OT-MoS_2 shows the redshift. One possible explanation to this phenomenon is the charge transfer effect. **Figure 4** gives the schematic illustration of the relative energy level between the ground and excited states of the R6G molecule and the electronic bands of MoS_2 at the low-energy regime. It can be seen that the top of valence band of MoS_2 is much lower compared to the excited state of R6G. Furthermore, as the adsorption of oxygen in OT-MoS_2 gives rise to the p-doping induced band filling effect, the top of valence band is filled by holes. Thus it fulfills the condition to accept the photoinduced electrons from the excited states of R6G, which would result in a blueshift of PL position for OT-MoS_2. Furthermore, because the plasma bombardment induced removal of local atoms and the distortion of chemical bonds would break the original symmetry of MoS_2-crystal, the local dipoles can be formed on the surface of MoS_2 nanoflakes, as shown schematically in Figure 1a. The symmetry of R6G molecule system can be slightly changed by the interaction with local dipoles of T-MoS_2, resulting in the differences in the mode selection and finally enhancing the Raman signal of R6G.

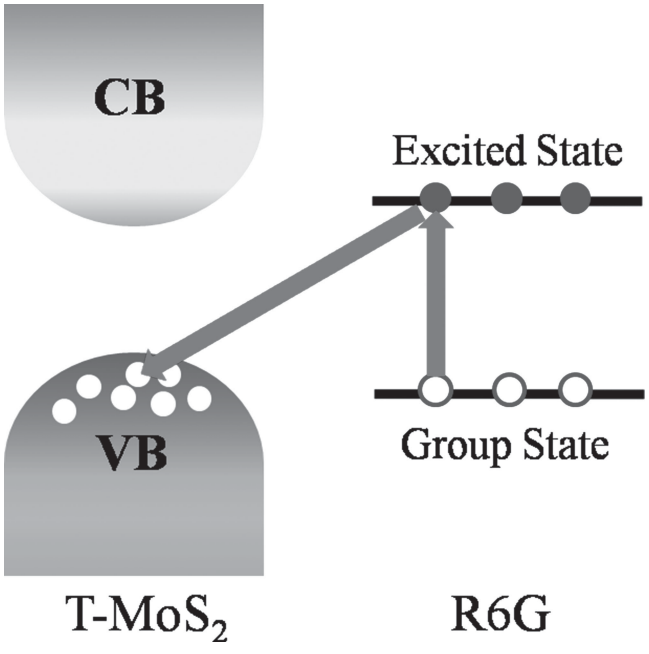

Figure 4. Schematic insulation of plasma enhanced photo-induced charge transfer between R6G molecular and T-MoS_2.

In addition to the 1L MoS_2 nanoflakes discussed above, SERS effects of R6G molecules on MoS_2 nanoflakes with the different thicknesses were also investigated for better understanding the MoS_2-based SERS mechanism. **Figure 5**a shows the optical image of a typical MoS_2 sample, including single layer (1L), bilayer (2L), trilayer (3L), multilayer (ML, where $5 < M < 10$) and bulk. The corresponding AFM image and its height profile are shown in Figure 5b to identify the layer numbers of MoS_2 nanoflakes.[29] The thicknesses were further confirmed by the Raman spectra (Figure 5c) in terms of the frequency difference between E^1_{2g} and A_{1g} modes, which is consistent to the reported values.[30,31] Figure 5d shows the Raman signals of R6G molecules deposited on OT-MoS_2 samples with the different thicknesses. Obviously, the Raman intensities of the R6G molecules are inversely proportional to the layer numbers of OT-MoS_2 nanoflakes as shown in Figure 5d. It is worth noting that the Raman signals of R6G molecules on bulk MoS_2 is very weak and it is almost invisible. Three possible factors may explain this thickness dependent Raman enhancement: (1) the layer dependent surface potential induced by the p-doping effect from SiO_2/Si substrate gives rise to the layer dependent SERS effect, which is just like the layer dependent SERS effect on different layered graphene samples.[32,33] (2) 2D material with more number of layers is more structurally stable against the electron/ion bombardment, resulting in generation of less amount of structural disorder. (3) The bandgap of MoS_2 depends on the number of layers, which also affect the band alignment and further has an effect on the charge transfer proposed in the model shown in Figure 4.[34,35] To find out the dominant factors, we specifically investigate the Raman spectra of R6G molecules on suspended OT-MoS_2 nanoflakes to examine whether this

NANO MICRO small

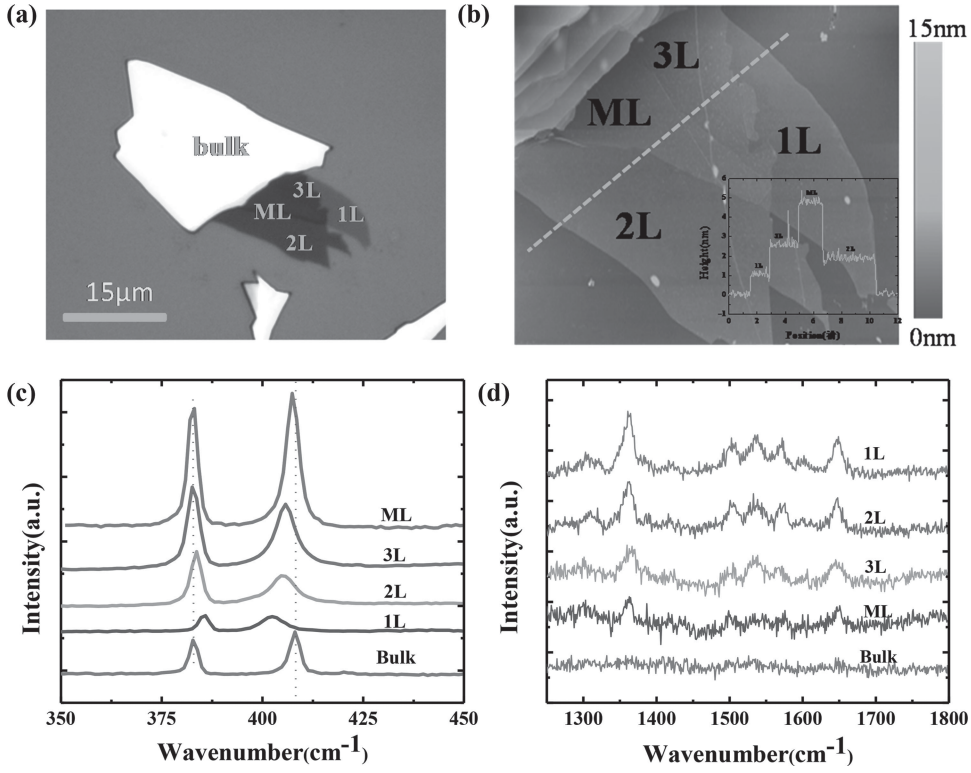

Figure 5. a) Optical image of a typical MoS_2 nanoflake deposited on SiO_2/Si. b) AFM image of MoS_2 nanoflake and its corresponding height profile. c) Raman spectra of OT-MoS_2 nanoflake, including 1L, 2L, 3L, ML and bulk. d) Raman spectra of R6G molecules on OT-MoS_2 samples with different thickness (baseline is subtracted in each spectrum).

layer-dependent enhancement effect in MoS_2 nanoflakes is related to the SiO_2/Si substrate (the proposed first factor). As shown in **Figure 6**, the 2L, 4L, ML, and bulk OT-MoS_2 samples are analyzed for studying the overall trend on the layer-dependent SERS effect. It is found that the trend of layer-dependent SERS effect for suspended OT-MoS_2 nanoflakes (Figure 6b) is similar as that for SiO_2/Si substrate supported OT-MoS_2 nanoflakes (Figure 5d), which indicates that the OT-MoS_2–based layer-dependent Raman enhancement for R6G is not caused by SiO_2/Si-substrate induced different surface potentials among different layered MoS_2 samples. Therefore, we propose that the decreased Raman enhancement factor with increasing thickness of OT-MoS_2 is mainly due to the rest two proposed factors, which are the less amount of structural disorder created (corresponding to the less amount of local dipoles introduced) in thicker MoS_2 nanoflakes, as well as the different band alignment. While Raman spectra of P-MoS_2 and OT(AT)-MoS_2 nanoflakes shown in Figure S3a (2L) and S3c (3L) also support this conclusion. Combined with the Raman spectra of 1L P-MoS2 and OT(AT)-MoS_2 shown in Figure 2a, it is clearly seen that the plasma treatment induced frequency variation for both E^1_{2g} and A_{1g} modes of MoS_2 decreases with increasing number of layers. Furthermore, comparing the PL peak position between P-MoS_2 and OT(AT)-MoS_2 in 1L (Figure 2b), 2L (Figure S3b) and 3L (Figure S3d), it is clearly seen that the PL blueshift effect of OT(AT)-MoS_2 decreases with increasing the thickness. Thus, both the Raman and PL results give evidence that under same plasma treatment condition, the structural disorders decreases with increasing

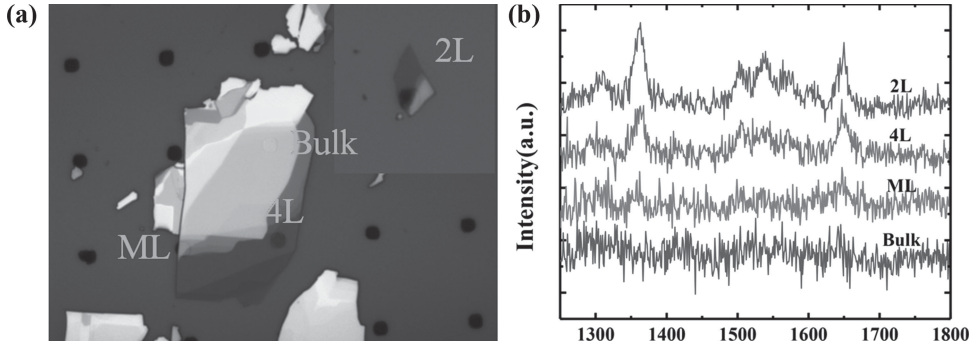

Figure 6. a) Optical images of suspended MoS_2 with different thicknesses (4L, ML and bulk), and the inserted image is suspended 2L MoS_2. b) Raman spectra of R6G on suspended OT-MoS_2 nanoflakes with different thickness (baseline is subtracted in each spectrum).

the thickness of MoS_2 nanoflakes.[18–20] Therefore, the less amount of structural disorder introduced in relatively thicker MoS_2 nanoflake gives rise to the less amount of induced local dipoles, and hence the overall SERS effect becomes weaker.

Plasma treated MoS_2 nanoflakes for surface enhanced Raman scattering of R6G molecule is reported. By systematically studying the Raman and PL spectra of both P-MoS_2 and OT(AT)-MoS_2 samples, it is proved that the structural disorders are created by the plasma bombardment process, resulting in the generation of local dipoles and adsorption of oxygen in ambient air. The adsorption of oxygen decreases the electron occupation level at the top of valence band of MoS_2, and hence it enhances the photoinduced charge transfer between R6G and MoS_2, as a consequence, the fluorescence of R6G is dramatically suppressed. While the generation of the local dipoles enhances the Raman signals of R6G due to the change of symmetry. Furthermore, both SiO_2/Si-supported and suspended T-MoS_2 samples show similar layer-dependent Raman enhancement trend, indicating that Raman enhancement factor has no relationship with the SiO_2/Si substrate induced surface potential, but it is determined by the amount of structural disorder generated during plasma treatment. The investigation of the interaction between MoS_2 (both P-MoS_2 and OT(AT)-MoS_2) and organic molecules through the SERS effect paves a new way for the potential practical applications, such as using OT(AT)-MoS_2 nanoflakes for molecule detection and biological detection.

Experimental Section

In our experiments, MoS_2 nanoflakes were exfoliated by the scotch tape from a nature MoS_2 crystal (SPI Supplies). The prepared samples treated by oxygen (argon) plasma with a constant oxygen (argon) flow maintained at 80 sccm for 5 seconds, and then the samples were soaked in 10^{-6} mol/L R6G molecules solution for 2 hours. Another group of pristine MoS_2 nanoflakes was taken for reference. The holes on the surface of SiO_2/Si with diameter of ~3 μm and the depth of ~500 nm for measuring the suspended MoS_2 samples were etched by the photolithography method. The Raman spectra were excited by a 532 nm laser line and conducted using Renishaw Raman Microscopy configured with a charge coupled device array detector. The power of the excitation laser was kept below 0.5 mW. The Raman signals were collected by a Leica 100 × objective lens (NA = 0.85) and dispersed by 2400 line mm^{-1} gratings with frequency resolution of ~0.8cm^{-1}. The PL measurement was performed on a WITEC CRM200 Raman system using a 532 nm laser as the excitation source with 150 line mm^{-1} grating.

Supporting Information

Supporting Information is available from the Wiley Online Library or from the author.

[1] B. Radisavljevic, A. Radenovic, J. Brivio, V. Giacometti, A. Kis, *Nat. Nanotechnol.* **2011**, *6*(3), 147–150.
[2] H. Wang, L. Yu, Y.-H. Lee, Y. Shi, A. Hsu, M. L. Chin, L.-J. Li, M. Dubey, J. Kong, T. Palacios, *Nano Lett.* **2012**, *12*(9), 4674–4680.
[3] Y. Yoon, K. Ganapathi, S. Salahuddin, *Nano Lett.* **2011**, *11*(9), 3768–3773.
[4] H. Li, Z. Yin, Q. He, H. Li, X. Huang, G. Lu, D. W. H. Fam, A. I. Y. Tok, Q. Zhang, H. Zhang, *Small* **2012**, *8*(1), 63–67.
[5] Q. He, Z. Zeng, Z. Yin, H. Li, S. Wu, X. Huang, H. Zhang, *Small* **2012**, *8*(19), 2994–2999.
[6] H. Hwang, H. Kim, J. Cho, *Nano Lett.* **2011**, *11*(11), 4826–4830.
[7] K. Chang, W. Chen, *ACS Nano* **2011**, *5*(6), 4720–4728.
[8] J. Xiao, D. Choi, L. Cosimbescu, P. Koech, J. Liu, J. P. Lemmon, *Chem. Mater.* **2010**, *22*(16), 4522–4524.
[9] D. Xiao, G.-B. Liu, W. Feng, X. Xu, W. Yao, *Phys. Rev. Lett.* **2012**, *108*(19), 196802.
[10] L. Sun, J. Yan, D. Zhan, L. Liu, H. Hu, H. Li, B. K. Tay, J.-L. Kuo, C.-C. Huang, D. W. Hewak, P. S. Lee, Z. X. Shen, *Phys. Rev. Lett.* **2013**, *111*(12), 126801.
[11] Y. Li, H. Wang, L. Xie, Y. Liang, G. Hong, H. Dai, *J. Am. Chem. Soc.* **2011**, *133*(19), 7296–7299.
[12] Q. Xiang, J. Yu, M. Jaroniec, *J. Am. Chem. Soc.* **2012**, *134*(15), 6575–6578.
[13] Y. Kim, J.-L. Huang, C. M. Lieber, *Appl. Phys. Lett.* **1991**, *59*(26), 3404–3406.
[14] F. K. Perkins, A. L. Friedman, E. Cobas, P. M. Campbell, G. G. Jernigan, B. T. Jonker, *Nano Lett.* **2013**, *13*(2), 668–673.
[15] R. Lv, Q. Li, A. R. Botello-Méndez, T. Hayashi, B. Wang, A. Berkdemir, Q. Hao, A. L. Elías, R. Cruz-Silva, H. R. Gutiérrez, Y. A. Kim, H. Muramatsu, J. Zhu, M. Endo, H. Terrones, J.-C. Charlier, M. Pan, M. Terrones, *Sci. Rep.* **2012**, *2*.
[16] S. Huh, J. Park, Y. S. Kim, K. S. Kim, B. H. Hong, J.-M. Nam, *ACS Nano* **2011**, *5*(12), 9799–9806.
[17] X. Yu, K. Lin, K. Qiu, H. Cai, X. Li, J. Liu, N. Pan, S. Fu, Y. Luo, X. Wang, *Carbon* **2012**, *50*(12), 4512–4517.
[18] G. Eda, H. Yamaguchi, D. Voiry, T. Fujita, M. Chen, M. Chhowalla, *Nano Lett.* **2011**, *11*(12), 5111–5116.
[19] Y. Zhan, Z. Liu, S. Najmaei, P. M. Ajayan, J. Lou, *Small* **2012**, *8*(7), 966–971.
[20] K.-K. Liu, W. Zhang, Y.-H. Lee, Y.-C. Lin, M.-T. Chang, C.-Y. Su, C.-S. Chang, H. Li, Y. Shi, H. Zhang, C.-S. Lai, L.-J. Li, *Nano Lett.* **2012**, *12*(3), 1538–1544.
[21] A. Castellanos-Gomez, M. Barkelid, A. M. Goossens, V. E. Calado, H. S. J. van der Zant, G. A. Steele, *Nano Lett.* **2012**, *12*(6), 3187–3192.
[22] C.-L. Hsiao, H.-C. Hsu, L.-C. Chen, C.-T. Wu, C.-W. Chen, M. Chen, L.-W. Tu, K.-H. Chen, *Appl. Phys. Lett.* **2007**, *91*(18), 181912.
[23] E. Monaico, V. V. Ursaki, I. M. Tiginyanu, Z. Dashevsky, V. Kasiyan, R. W. Boyd, *J. Appl. Phys.* **2006**, *100*(5), 053517.
[24] M. Strassburg, A. Hoffmann, J. Holst, J. Christen, T. Riemann, F. Bertram, P. Fischer, *Phys. Status Solidi (c)* **2003**, *0*(6), 1835–1845.
[25] F. Qian, Y. Li, S. Gradecak, H.-G. Park, Y. Dong, Y. Ding, Z. L. Wang, C. M. Lieber, *Nat Mater* **2008**, *7*(9), 701–706.
[26] S. Ryu, L. Liu, S. Berciaud, Y.-J. Yu, H. Liu, P. Kim, G. W. Flynn, L. E. Brus, *Nano Lett.* **2010**, *10*(12), 4944–4951.
[27] Z. Zhang, J. T. Yates, *Chem. Rev.* **2012**, *112*(10), 5520–5551.
[28] Y. Yan, Z.-M. Liao, Y.-Q. Bie, H.-C. Wu, Y.-B. Zhou, X.-W. Fu, D.-P. Yu, *Appl. Phys. Lett.* **2011**, *99*(10), 103103.
[29] E. S. Kadantsev, P. Hawrylak, *Solid State Commun.* **2012**, *152*(10), 909–913.
[30] C. Lee, H. Yan, L. E. Brus, T. F. Heinz, J. Hone, S. Ryu, *ACS Nano* **2010**, *4*(5), 2695–2700.

[31] H. Li, Q. Zhang, C. C. R. Yap, B. K. Tay, T. H. T. Edwin, A. Olivier, D. Baillargeat, *Adv. Funct. Mater.* **2012**, *22*(7), 1385–1390.
[32] X. Ling, L. Xie, Y. Fang, H. Xu, H. Zhang, J. Kong, M. S. Dresselhaus, J. Zhang, Z. Liu, *Nano Lett.* **2009**, *10*(2), 553–561.
[33] S. S. Datta, D. R. Strachan, E. J. Mele, A. T. C. Johnson, *Nano Lett.* **2008**, *9*(1), 7–11.
[34] A. Castellanos-Gomez, E. Cappelluti, R. Roldán, N. Agraït, F. Guinea, G. Rubio-Bollinger, *Adv. Mater.* **2013**, *25*(6), 899–903.
[35] Y. Li, C.-Y. Xu, L. Zhen, *Appl. Phys. Lett.* **2013**, *102*(14), 143110.

Received: March 13, 2013
Revised: October 26, 2013
Published online: February 13, 2014

